San L.Tolentino
Research
National Experimental Polytechnic University "AJS" (UNEXPO)
Bolívar
Venezuela
Research collaborator
Group of Mathematical Modeling and Numerical Simulation (GMMNS)
National University of Engineering (UNI)
Lima
Perú

Jorge Mírez
Elec. Mech, Eng.; MSc & Dr Physics
Professor
Group of Mathematical Modeling and Numerical Simulation (GMMNS)
National University of Engineering (UNI)
Lima
Perú

Omar González
Faculty of Civil Engineering
National University Hermilio Valdizán (UNHEVAL)
Huánuco
Perú

Evaluation of Turbulence Models for Incompressible Flow in a Venturi Tube

Turbulence models are semi-empirical transport equations that model flow behavior. They are compared on a recurring basis to know which of them presents the best fit with experimental data for different laboratory equipment. In the present work, the incompressible flow field (water) is simulated with the computational fluid dynamics (CFD) tool and RANS model for the geometry of a Venturi tube in 2D computational domains, with the objective of evaluating six turbulence models: standard k-ε, RNG k-ε, standard k-ω, SST k-ω, RSM and SA. The numerical results of the trajectories of the pressure pattern curves at the walls and axial symmetry are close to each other. Pressure drops occur at the throat. The percentage errors of the turbulence models increase as the magnitude of the pressure ratio increases, for r_p=1.0932, r_p=1.1118, r_p=1.1377, and r_p=1.1531. It is concluded that the SA turbulence model of Spalart-Allmaras (1992) best fits the experimental pressure data, with percentage errors of less than 10%.

Keywords: *Incompressible flow, pressure patterns, Turbulence models, Venturi tube, Computational fluid dynamics.*

1. INTRODUCTION

The Venturi tube is a flow meter invented by Clemans Herschel [1] and named "Venturi tube" in honor of Gio–vanni B. Venturi for his early contributions to flow in conic sections [2]. It has multiple applications in industrial pro–cesses, aerospace, and automotive [3-5], among other areas.

The ASME text [6] details the instruments that measure a fluid's flow rate, which are classified as mechanical instruments and head loss instruments. The Venturi tube is found as a pressure loss instrument by vein contraction [2].

There are different geometric configurations of the Venturi tube, which are mentioned in some studies carried out for incompressible flow [7-9]. For compressible flow [9-11], as well as for multiphase flow and liquid and gas interaction [12-15]. The turbulence of the flow and the gradients of pressure and temperature, among others, are different for each case, as well as the behavior of the boundary layer, the flow separation, and the lateral pressure loads [16]. By means of the ratio of inertia forces and viscous forces, the Reynolds number is calculated as a dimensionless parameter, which determines whether the flow is laminar or turbulent [2,17].

The throat section of the Venturi tube has the lowest pressure drop. Its gradual contraction and expansion decrease flow separation and eddies, and frictional losses occur at the inner wall surfaces, where the irreversible pressure drop due to friction for Venturi meters is around 10% [2]. However, under certain conditions of the pressure field, the pressure can reach values lower than the vapor pressure. Thus, cavitation occurs [18-20]. Also, cavitation-induced choked flow occurs in liquids with a gas mixture [21].

During the experiments, flow pressure readings on the walls are only possible at local points. Recording experi–mental data in critical sections, such as at the edges, where the section changes of the device geometry occur, is difficult.

With the use of computational fluid dynamics (CFD) [22,23], it is possible to simulate the behavior of the flow for certain conditions of the flow's thermodynamic parameters. CFD employs turbulence models, with so–me expressed with a single equation and others with two equations. The turbulence models act as a closure to the Reynolds-Averaged Navier-Stokes (RANS) equations [23].

Based on the choice of a suitable turbulence model, the numerical results of computational simulations in the area of fluid mechanics can satisfactorily appro–ximate the flow field of the physical phenomenon under study for any geometry of different dimensions. Provided that certain established numerical error margin criteria are met. Since errors accumulate due to different causes, such as modeling errors, discretization errors, iteration errors, and programming and user errors [22], it should be noted that the deviations of the percentage errors depend very much on the method of discretization of the computational domain, either by the finite volume method (FVM), finite element method (FEM), finite difference method (FDM), or other methods. As well as by the meshing structured by triangular cells, quadrilateral cells, or other types of cells.

Tolentino addressed studies for incompressible flow (water) in a Venturi tube [7]. The flow was simulated with the COMSOL Multiphysics v4.3 code that applies the FEM for 2D computational domains and meshed with quadrilateral cells for the standard k - ε [24] and standard k - ω [25] turbulence models.Numerical results for both turbulence models presented negative pressures in the

Received: June 2024, Accepted: August 2024
Correspondence to: Dr. Jorge Mírez, Group of Mathematical Modeling and Numerical Simulation, National University of Engineering (UNI), Lima, Perú
E-mail: jmirez@uni.edu.pe
doi: 10.5937/fme2404534T

throat section for pressure ratios r_p = 1.1377 and $_p$ = 1.1531.

Studies reported by Tolentino et al. [26] for the same Venturi tube geometry reported in [7] employed the ANSYS-Fluent R16.2 code that applies the FVM. The incompressible flow (water) was simulated in 2D discretized domains with quadrilateral cells for the hybrid Scale-Adaptive Simulation (SAS) and Detached Eddy Simulation (DES) models [23]. They obtained numerical results in the throat section of positive pressures for r_p = 1.1377 and $_p$ = 1.1531. The difference in the numerical results is evident for both cases of studies reported in [7] and [26].

Li et al. [27] addressed the study of incompressible flow in a Venturi tube on hydrodynamic cavitation for the generation of microbubbles. The flow simulation was with the standard k - ω turbulence model [25], with the COMSOL Multiphysics code. Due to the applied pressure conditions in the throat section, the pressure drops are negative.

Other numerical studies applying CFD for the simulation of the flow field in Venturi tube geometries and comparing it with experimental data were addressed by Kim et al. [12] with the SST k - ω model [27]. Tukimin et al. [11], Zhang et al. [13], Sun [28], and Youlin et al. [29] simulated the flow with the standard k - ε turbulence model [24].Also, for the calibration of the Venturi tube, twenty-one cases of different geometries for incompressible and compressible flow have been addressed by Reader et al. [30]. Also, some relevant studies on the flow behavior for different turbulence models applied in other geometries are mentioned, such as flow simulations in a small bulb turbine [31], geometric analysis of turbulent macrostructure [32], analysis of turbulence intensity [33], non-equilibrium boundary layer [34], turbulence model of atmospheric boundary layer [35], and evaluation of turbulence models for the airflow [36], [37].

It should be noted that the choice of the turbulence model to model the turbulence of the flow, without having been validated, is likely to present high deviations of numerical errors. Therefore, the numerical results would be far from the reality of the physical phenomenon. That is why evaluating different turbulence models and validating them with experimental data is important. In the area of fluid mechanics for incompressible flow, turbulence models have applications to simulate internal and external flow behavior, such as the simulation of flow in different configurations of hydraulic turbines, pipe network systems, counter-flow cooling systems, and liquid reservoirs, among others.

In the present work,for incompressible flow, the objective is to evaluate six turbulence models, namely: standard k - ε of Launder and Spalding [24], RNG k - ε of Orszag et al. [38], standard k - ω of Wilcox [25], SST k - ω of Menter [27], RSM of Launder et al. [39], and SA of Spalart-Allmaras [40], in order to determine which of the turbulence models exhibits the lowest numerical error and best fits the experimental pressure data. The turbulence models are simulated for incompressible flow (water) in 2D computational domains for the geometry of a Venturi tube. It should be noted that the calculations of Reynolds numbers and discharge coefficients are out of the scope of the study since they are reported in [7], [26]. Section 2 presents the methodology. Section 3 presents the results of the evaluations of the six turbulence models, which are compared with experimental pressure data. Also, the flow field simulations with the selected turbulence model are presented. Then, in section 4, the conclusions of the analysis are presented.

2. METHODOLOGY

2.1 Laboratory equipment: Venturi tube

Fig. 1 (a) shows the Venturi tube used for experimental flow measurements by pressure differences for incompressible flow (water). The laboratory equipment is installed in the Thermofluids section of the Mechanical Engineering Department of the UNEXPO "AJS", Puerto Ordaz, Bolivar, Venezuela. This flow measurement device with a convergent-divergent and straight-cut throat section is designed and manufactured by the TecQuipment company.

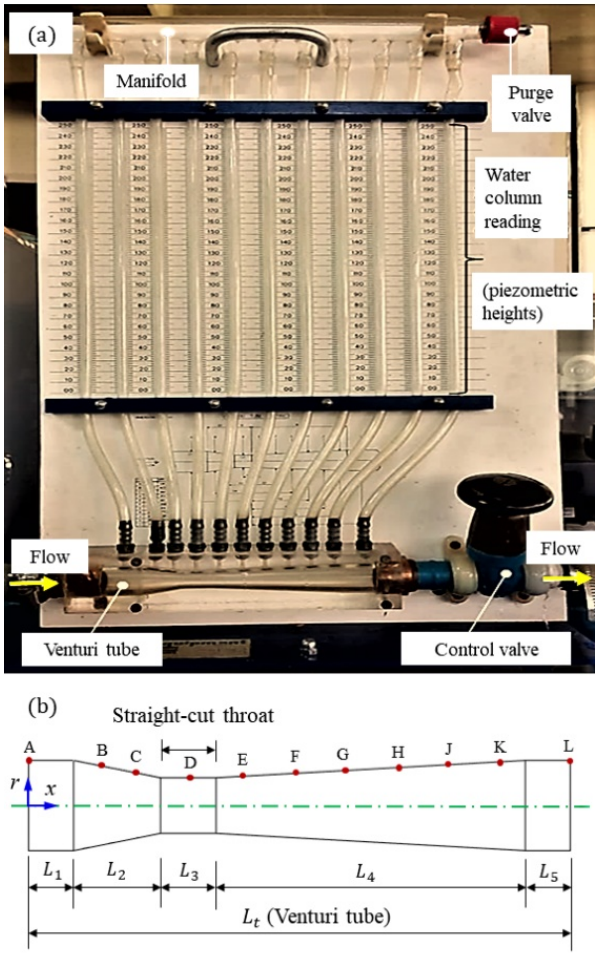

Figure 1. (a) Laboratory equipment: Venturi tube. (b) Schematic of the Venturi tube showing the positions of the references from A to L, which correspond to the locations of the connections of the piezometric tubes.

Eleven transparent plastic hoses, known as piezometric tubes, are connected to the walls of the Venturi tube. The hose connections are distributed at local points identified by the references A, B, C, D, E, F, G, H, J, K, and L (Fig. 1(b)), which measure the water column pressure in units of millimeters (piezometric heights).

The flow study section starts at reference A and ends at reference L. The dimensions of the Venturi tube section, as well as the positions of the eleven hoses for the gauge pressure readings, are presented in Table 1.

Table 1. Reference positions from A to L, diameter dimensions, and lengths of Venturi tube sections.

Ref.	Diameter (mm)	Position (mm)	Position x/L_2
A	26.0	0.0	0.0
B	23.2	20	0.1282
C	18.4	32	0.2051
D	16.0	46	0.2948
E	16.8	61	0.3910
F	18.47	76	0.4871
G	20.16	91	0.5833
H	21.84	106	0.6794
J	23.53	121	0.7756
K	25.24	136	0.8717
L	26.0	156	1.0
Length(mm)			
L_1	L_2	L_3	L_4	L_5
13	25	16	89	13

Tolentino [7] reported five experimental manometric pressure tests in units of millimeters of water (mmH2O) for the references from A to L (Fig. 1). Of which, four pressure tests (experiments 2, 3,4, and 5) are taken into consideration in the present work. The same is presented in Table 2, with the purpose of comparing with the pressure data six turbulence models reported in the literature. Experiment 1 has yet to be included due to limitations in the investigation since it presents smaller pressure jumps with respect to experiments 2,3,4, and 5.

Table 2. The flow rate, Reynolds number, and gauge pressures of the water columns were evaluated at the Venturi tube wall at local points (references from A to L), as reported by Tolentino [7].

Exp.	2	3	4	5
	Flowx10^4 (m^3/s)			
	2.583	2.991	3.382	3.704
Ref.	Reynolds number			
A	13839	16028	18118	19844
D	22489	26045	29442	32246
Ref.	Gauge pressure (mmH_2O)			
A	170	179	190	199.5
B	165	172	181	189
C	139.5	139.5	139.5	139.5
D	91	76.5	60.5	45
E	97	85	72	60
F	122	119	115.5	112
G	136	136	136	136
H	144.5	146.5	150	152
J	149.5	153	158	162
K	153	157.5	163.5	168.5
L	155.5	161	167	173

2.2 Computational domain and meshing

Fig. 2 (a) illustrates the computational domain of the 2D Venturi tube geometry. The same figure shows where the boundary conditions are applied. It should be noted that 2D computational domains were considered because of the symmetry of the Venturi tube geometry in the radial direction. Also, 2D computational domains save data processing time compared to 3D domains.

The 2D domain was meshed with quadrilateral cells, in the ANSYS-Meshing platform using ICEM-CFD interaction to discretize the domain, which is shown in Fig. 2(b). The mesh was refined toward the walls by the effect of flow shear stresses in regions adjacent to the walls. A magnification detail of the straight-cut throat section and its ends is shown in Fig. 2(c), where the distribution of the refined cells in the regions adjacent to the walls can be observed.

The magnitudes of pressure and velocity parameters of boundary conditions are presented in Table 3, where, the pressure ratio $r_p = P_{inlet}/P_{outlet}$ are tabulated for experiments 2, 3, 4, and 5, which were evaluated for water temperature at 24°C, for isothermal flow conditions, being the density of water ρ = 997.1015 kg/m^3 and of dynamic viscosity μ = 9.1135x10^{-4}·N s/m^2.It should be noted that, as the flow velocity at the inlet of the Venturi tube is taken into consideration, it is no longer necessary to include the mass flow. This is because the pressure-based flow type was taken into account in the ANSYS-Fluent code.

The walls of the Venturi tube are considered adia–batic, and the flow velocity on the walls is considered to be zero due to the flow's no-slip condition. On the axis of symmetry, in the radial direction, the flow velocity is zero. The effect of gravity on the flow inside the Venturi tube is not taken into account since the pressure gradient of the flow is considered to act in the radial direction.

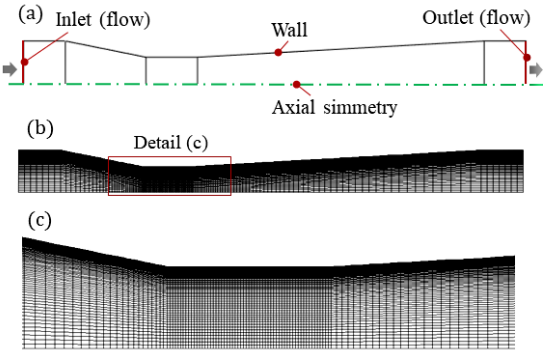

Figure 2. (a) 2D domain, in which the boundary conditions are indicated. (b) Structured grid with quadrilateral cells, with a total of 12300 elements. (c) Enlarged detail of the straight-cut throat section.

Table 3. Parameters of the boundary conditions at the inlet and outlet of the Venturi tube.

Exp. [7]	Inlet		Outlet	r_p
	Velocity (m/s)	Pressure (mmH_2O)	Pressure (mmH_2O)	
2	0.4865	170	155.5	1.0932
3	0.56335	179	161	1.1118
4	0.63699	190	167	1.1377
5	0.69764	199.5	173	1.1531

2.3 Mathematical fundamentals

For the simulation of the incompressible flow field with the ANSYS-Fluent R16.2 code applying the FVM [22], [23] for steady-state conditions, the equations of the

RANS model have been used. Equation (1) of mass conservation and equation (2) of momentum. In com–pact form, they are expressed as:

$$\nabla \cdot (\rho u_i) = 0 \tag{1}$$

where ρ is the density, and u is the velocity.

$$\nabla \cdot (\rho u_i u_j) = -\nabla p + \nabla \cdot (\bar{\bar{\tau}}) + \nabla \cdot (-\rho \overline{u_i' u_j'}) \tag{2}$$

where p is the pressure, $\bar{\bar{\tau}}$ is the stress tensorandis expressed as $\bar{\bar{\tau}} = \mu \left[(\nabla u_i + \nabla u_j) - \frac{2}{3} \delta_{ij} \nabla \cdot u_l \right]$, where μ is the molecular viscosity, l is the unit tensor, δ_{ij} is the Kronecker delta, if i and j are equal their value is one, if they are different, their value is zero. As well as $-\rho \overline{u_i' u_j'}$ is the Reynolds stress.

Turbulence models have been developed to simulate flow turbulence under adverse pressure and boundary layer separation conditions. Turbulence models are semi-empirical transport equations that model mixing and diffusion enhanced by turbulent eddies as a function of fluid viscosity and turbulent viscosity, among other variables [23].

The six turbulence models used in the computational simulations in the present work are as follows: standard $k - \varepsilon$ of Launder and Spalding [24], RNG $k - \varepsilon$ of Orszag et al. [38], standard $k - \omega$ of Wilcox [25], SST $k - \omega$ of Menter [27], RSM of Launder et al. [39], and SA of Spalart-Allmaras [40]. Their noted authors report the mathematical foundations of the turbulence models in the literature.

The percentage error, e, is determined by the expre-ssion $e = |(p_{exp}\text{-}p_{sim})/p_{exp}|x100$. Where p_{exp} is the pressure from experimental data, and p_{sim} is the pressure from computational simulations.Thus, the sum of the quadratic error is expressed as $\Sigma e^2 = (p_{exp} - p_{sim})^2$.

2.4 Computational solution method

Different options were considered for the computational solution method in the ANSYS-Fluent R16.2 code. Type: pressure-based; Time: steady. 2D space: axisym–metric. Scheme: SIMPLE. Gradient: Least squares cell based. Pressure, momentum, andmodified turbulent viscosity: second-order upwind. Initialization methods: hybrid. For the control of the residual monitor, $1x10^{-7}$ was taken into account for continuity and speed. The numerical calculations of the computational simulations are in the range of 761-3572 iterations.The following computer equipment was used for data processing: Dell CPU, model Optiplex 7010, i5 3470. Four processors of 3.2 GHz and 8 Gb of RAM.

2.5 Numerical convergence analysis

Numerical convergence analysis was performed for three mesh densities. being mesh 1 with 10660 elements, mesh 2 with 11480 elements and mesh 3 with 12300 elements. The incompressible flow was simulated for r_p = 1.0932 with the SA turbulence model of Spalart-Allmaras [40].

The results of the curves of y^+ in shear stress value for the three meshed domains are shown in Fig. 3(a), with the curve for mesh 3 having values of $y^+ < 1.19$. For the wall shear stress curves of mesh 1, mesh 2, and mesh 3, shown in Fig. 3(b), are all superimposed.

No matter how much the mesh density is increased, the value of wall shear stress does not change in magnitude. For r_p = 1.0932, the mass flow obtained by numerical simulation is 0.25755 kg/s, while the experimental one is 0.257551 kg/s [7], [26], which yields a percentage error of $3.88x10^{-4}$. Therefore, the optimal meshing corresponds to mesh 3, which has 12300 elements used in the present work's flow field simulations and is the same meshed 2D domain shown above in Fig. 2(b). It should be noted that the numerical results are slightly affected by internal and incompressible flow in devices with symmetric wall geometries. In contrast, for non-symmetric geometries, the turbulence and flow separation computational domains imply a further increase of the cell density in the critical regions in order to reduce the numerical errors of the thermodynamic flow parameters.

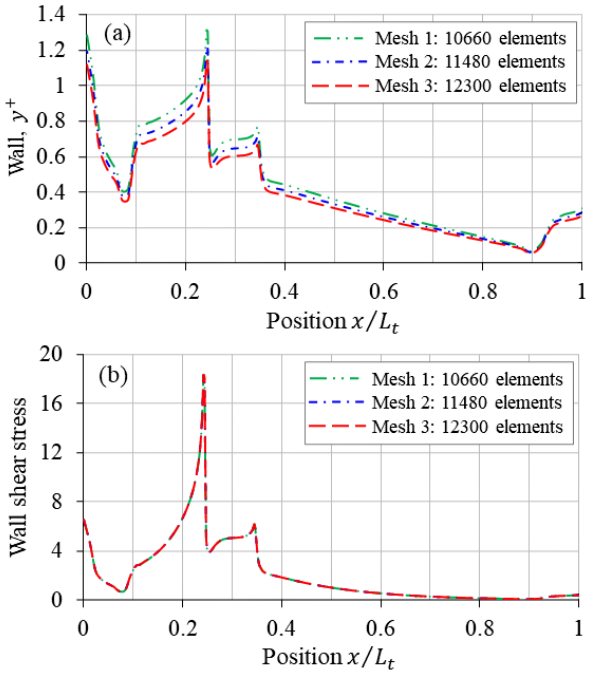

Figure 3. (a) Curvedpaths of y^+in shear stress value. (b)Curvedpaths of wall shear stress.

3. RESULTS AND DISCUSSION

In this section, the results of numerical simulations for six turbulence models are presented and compared with experimental pressure data. Next, the pressure field simulations obtained with the SA turbulence model of Spalart-Allmaras [40] are presented.

3.1 Theoretical predictions compared with experi–mental data

The curve trajectories of the standard $k - \varepsilon$ [24], RNG $k - \varepsilon$ [38], standard $k - \omega$ [25], SST $k - \omega$ [27], RSM [39], and SA [40] turbulence models are shown in Fig. 4, which are compared with experimental pressure data reported by Tolentino [7], for pressure ratios r_p =

1.0932, r_p = 1.1118, r_p = 1.1377 and r_p = 1.1531, respectively. The trajectories of the turbulence model curves have similar behavior as the pressure ratio r_p increases.

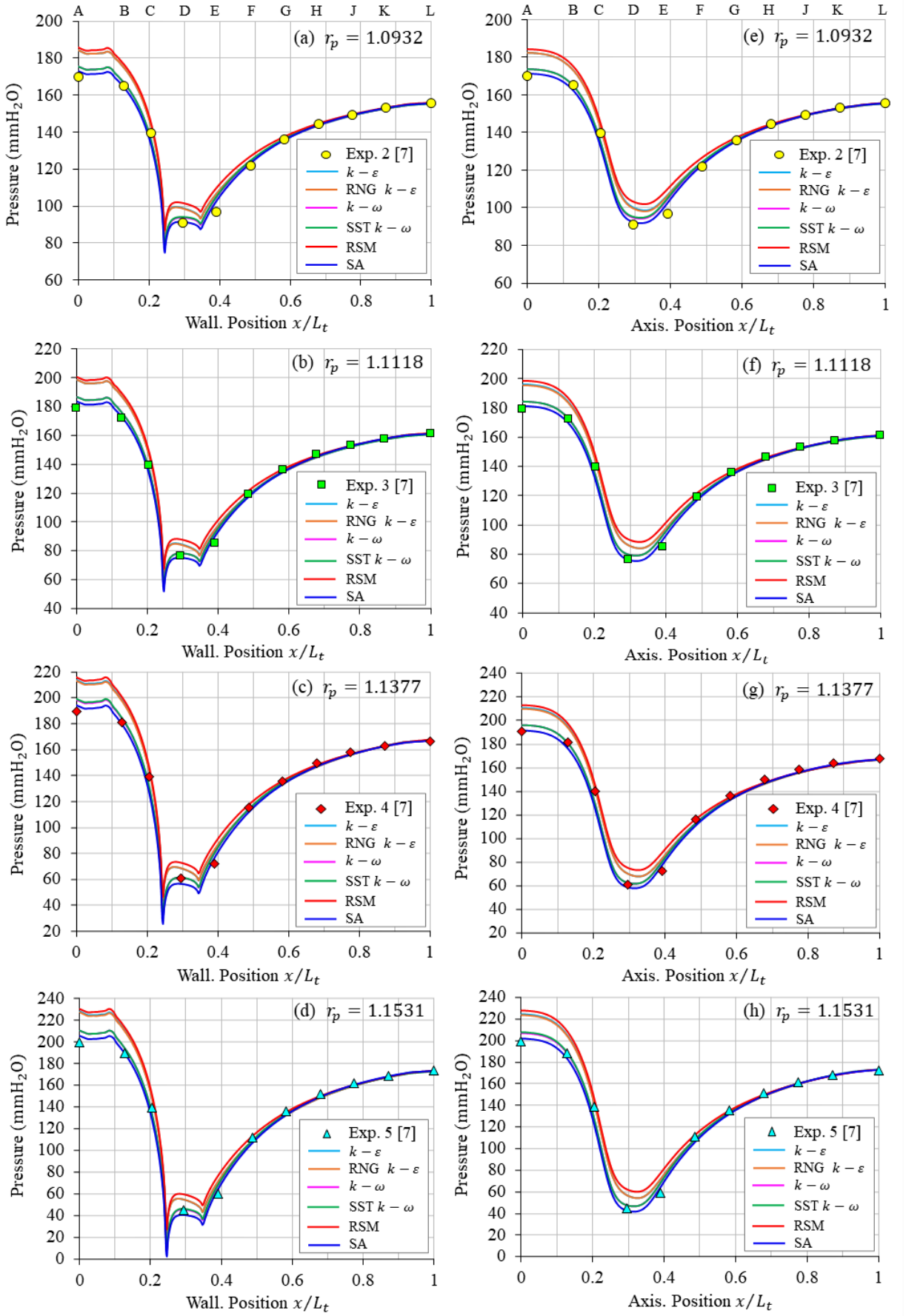

Figure 4. Comparison of curve trajectories from numerical simulations for six turbulence models with experimental pressure data [7]. (a)-(d) Pressure patterns at the wall. (e)-(h) Pressure patterns in axial symmetry.

The curves of the standard $k - \varepsilon$, RNG $k - \varepsilon$, and RSM turbulence models are far from the experimental pressure data from reference A to G for the flow pressure at the wall (Fig. 4(a)-(d)) and at axial symmetry (Fig. 4(e)-(h)). Whereas, for the flow toward the Venturi tube outlet, the curves are closer to the experimental data from reference G to L. Also separated are the curves of the standard $k - \omega$ turbulence and SST $k - \omega$ models from the experimental pressure data from reference A to B. The rest of the trajectories of the curves are closer to the experimental data.

The SA turbulence model curve is closer to the experimental pressure data with respect to the other turbulence model curves.

For the flow at the Venturi tube inlet, at reference A, the numerical simulations of the turbulence models standard $k - \varepsilon$, RNG $k - \varepsilon$, RSM, standard $k - \omega$ and SST $k - \omega$ present larger deviation of pressure values with respect to the experimental data. While, towards the outlet of the Venturi tube, at reference L, the curves converge and conform to the experimental pressure data.

In the straight-cut throat section, reference D is found, the region where the lowest pressure drop of the flow occurs, both in the wall and in the axial symmetry. In the case of the wall at the ends of the throat that joins the convergent and divergent sections, the turbulence model curves show the lowest pressure drops with respect to reference D. As the pressure ratio r_p increases, the pressure decreases to values close to the suction pressure. In addition, in reference D, the flow velocity is higher with respect to the other references.

In the regions of references C and G, all the turbulence model curves have constant pressure values close to the experimental pressure data values of 139.5 mmH_2O (reference C) and 136 mmH_2O (reference G). There, in the C and G references, the pressures do not vary no matter how much the kinetic energy of the fluid increases. Therefore, the experimental pressure difference is constant at 3.5 mmH_2O, and this is only for the calibration in the initial state of the water columns of the piezometric tubes (references A to L) of 140 mmH_2O [7]. Therefore, if the curves of the turbulence models for r_p = 1.0932, r_p = 1.1118, r_p = 1.1377 and r_p = 1.1531, were superimposed, all the curves would be intercepted. Further on, only the case of the SA turbulence model are shown in Fig. 6.

The intercept of the curves is due to the fact that the flow control valve at the inlet of the Venturi tube is manipulated, while the flow control valve at the outlet of the Venturi tube remains with constant opening as the flow is discharged to a reservoir at local atmospheric pressure; whereas, the air in the manifold supports the water columns in the piezometric tubes. For this reason, manipulation of the valve at the Venturi inlet affects the piezometric columns and generates a higher pressure drop in the throat section [7].

On the other hand, if only the flow control valve at the outlet of the Venturi tube is manipulated and the flow control valve at the inlet of the Venturi tube remains with constant opening, the pressure drops in the throat section would be slight and different with respect to the results shown in Fig. 4.

Figure 5 shows the behavior of the trajectories of the percentage error curves of the turbulence models for the flow pressure at the Venturi tube walls, evaluated in references A, B, C, D, E, F, F, G, h, J, K, and L. It is observed that the turbulence models model the flow behavior with different percentage error deviations. As the pressure ratio r_p increases, the percentage of errors increases. It should be noted that Fig. 5 (a)-(d) is related to Fig. 4 (a)-(d).

In reference E, the RSM turbulence model presents the highest peak error of 12.82% for r_p = 1.0932, 16.58% for r_p = 1.1118, and 21.53% for r_p = 1.1377. While, for r_p = 1.1531, the highest error peak of 32.53% is presented in reference D.

The standard $k - \varepsilon$ and RNG $k - \varepsilon$ turbulence models have similar behaviors of curve trajectories. In reference E, a peak error of 9.77% for r_p = 1.0932, 12.01% for r_p = 1.1118, 15.02% for r_p = 1.1377 is presented. In reference D, the error is 21.76% for r_p = 1.1531.

Also, the standard $k - \omega$ turbulence and SST $k - \omega$ models have similar behaviors of curve trajectories, where, in reference D, the error is 8.15% for r_p = 1.0932, 9.73% for r_p = 1.1118, 11.78% for r_p = 1.1377 and 15.43% for r_p = 1.1531.

The SA turbulence model has a smaller percentage of errors than the other turbulence models that have been mentioned. And it fits more closely with the experimental pressure data. In reference E, the error is 5.8% for r_p = 1.0932, 6.33% for r_p = 1.1118. In reference C, the error is 8.26% for r_p = 1.1377 and 9.96% for r_p = 1.1531. Furthermore, the SA turbulence model presents the smallest magnitude of the squared error sum with a value of Σe^2 = 76.43 (Table 4). While, the other turbulence models present higher values.

Table 4. The sum of squared error for different turbulence models.

Turbulence models	Sum of squared error
Standard k - ε	496.13
RNG $k - \varepsilon$	474.69
Standard k - ω	118.71
SST k - ω	123.44
RSM	707.78
SA	76.43

Numerical results reported in [7] from simulations for incompressible flow with the COMSOL Multi–physics v4.3 code applying the FEM for the same Venturi tube rig shown in Fig. 1 show that the standard $k - \varepsilon$ turbulence model fits the experimental pressure data better with respect to the standard $k - \varepsilon$ turbulence model. However, for the flow at the throat inlet, the two turbulence models present negative pressures for r_p = 1.1377 and r_p = 1.1531. Furthermore, the two turbulence models mentioned above, when evaluated for computational domains with the ANSYS-Fluent R16.2 code that applies the FVM, present positive pressures (Fig. 4) and higher percentage errors in certain regions with respect to the SA turbulence model, as shown in Fig. 5.

Numerical studies reported in [26], on the comparison of hybrid DES and SAS models, simulated with ANSYS-Fluent R16.2, show that the DES-SA and DES

$k-\varepsilon$ hybrid turbulence models present better fit to the experimental pressure data, whereas, the two-hybrid turbulence models DES SST $k-\varepsilon$ and SAS present a slight deviation of the pressure magnitude at the Venturi tube inlet, in reference A. For the DES and SAS hybridturbulence models, the percentage errors based on the Reynolds number are less than 6.5% [26].

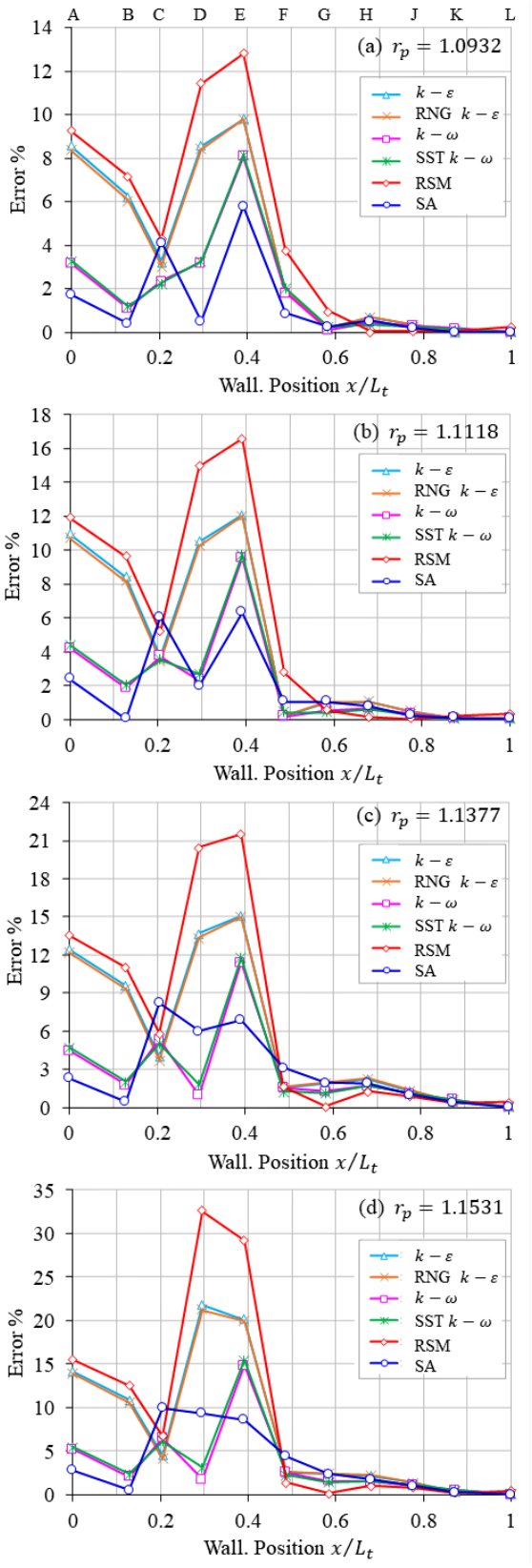

Figure 5. Percentage errors for different turbulence models for the flow pressure at the Venturi tube walls.

In that sense, the standard $k-\varepsilon$, RNG $k-\varepsilon$, standard $k-\omega$, SST $k-\omega$, RSM, and SA turbulence models present higher pressure deviances with respect to the DES and SAS hybrid turbulence models [26]. Whereas, in the present work, the SA turbulence model (Fig. 5) presents the maximum peak error of 9.96% in reference C for r_p = 1.1531, and in reference E presents the error of 5.8% for r_p = 1.0932. As well as, the standard $k-\varepsilon$, RNG $k-\varepsilon$, standard $k-\omega$, SST $k-\omega$, and RSM tur–bulence models present higher percentage errors (Fig. 5).

3.2 Numerical simulation with the SA turbulence model of Spalart-Allmaras

Numerical simulations with the SA turbulence model show the behavior of the trajectories of the pressure curves at the walls (Fig. 6(a)) and at the symmetry axis (Fig 6(b)), which are compared with experimental pressure data. As the pressure ratio r_p increases, inc–reasing pressures are observed at the ends of the Venturi tube in references A and L, as well as in the straight-cut throat section; in reference D, pressure drops are shown at the ends of the throat.

It is also observed that the curves converge in the regions of references C and G. There, at these two local points, the pressures are the same for all the curves, and the flow velocities are different. An enlarged detail between references C and G is shown in Fig. 7. The pressure behavior on the symmetry axis and on the walls of the Venturi tube is observed.

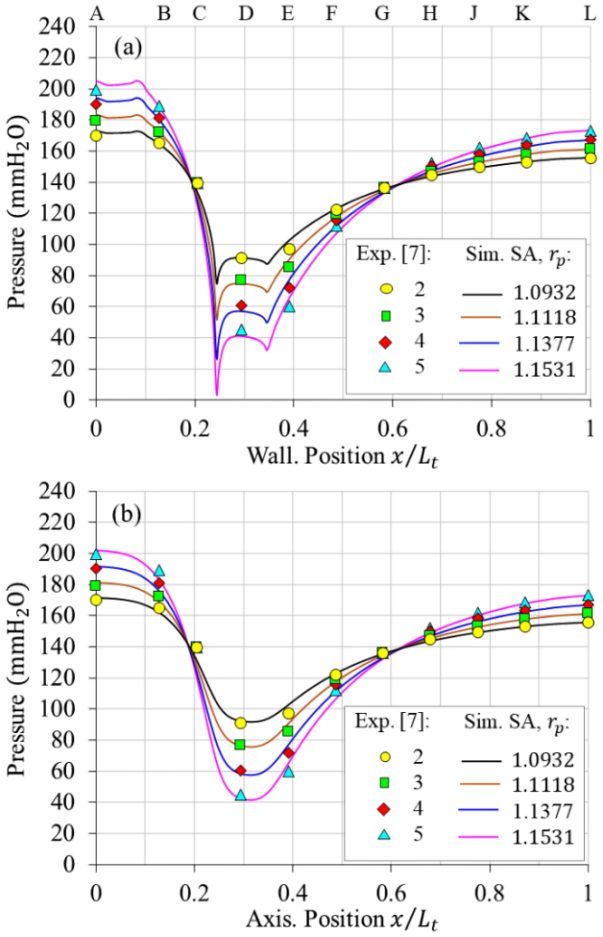

Figure 6. (a) Pressure patterns at the wall. (b) Pressure patterns in axial symmetry.

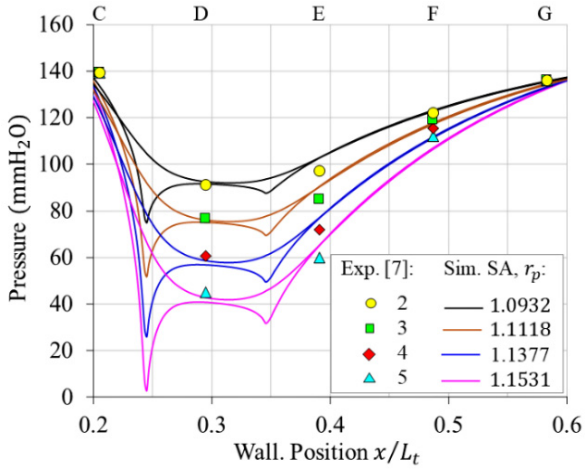

Figure 7. Trajectories of pressure curves at the wall and axial symmetry between references C and G.

The pressure (mmH_2O) field by contour lines is shown in Fig. 8. The pressure gradient distribution of the flow is observed in the central region and towards the walls of the Venturi tube, as well as at the ends of the straight-cut throat.

In the convergent, the pressure contour lines tend to curve in the radial direction. Whereas, in divergent ones, the pressure contour lines tend to be slightly smooth and parallel. The variations of the magnitudes of the wall pressures have been shown in Fig. 7(a), and the symmetry axis in Fig. 7(b). The variation in the percentage of errors is also shown in Fig. 5.

It should be noted that the numerical results of the different turbulence models used in the simulations of the incompressible flow field with the ANSYS-Fluent R16.2 code are approximations that present percentage error margins with respect to experimental pressure data. Therefore, the turbulence model with the lowest numerical error has been presented.

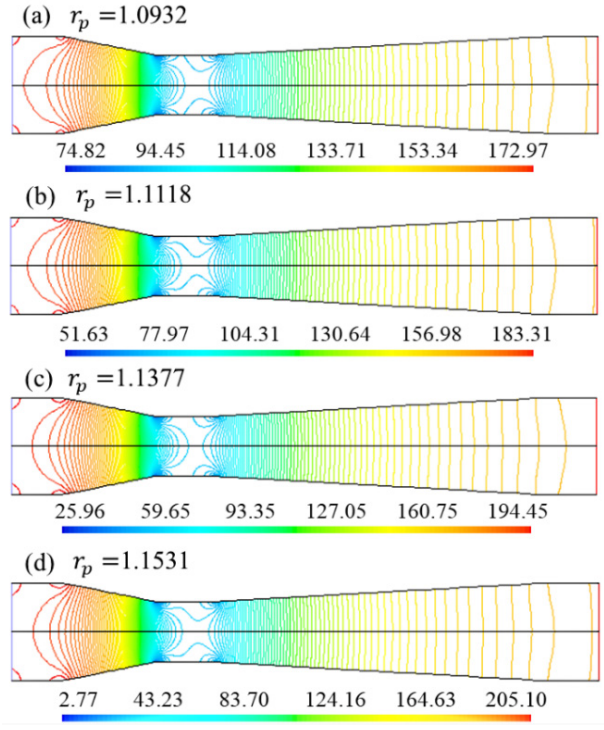

Figure 8. Contour line pressure field for different pressure ratios r_p.

4. CONCLUSIONS

Based on the analyses of the numerical results obtained for incompressible flow in a Venturi tube, the following is concluded:

As the magnitude of the pressure ratio increases, for r_p = 1.0932, r_p = 1.1118, r_p = 1.1377 and r_p = 1.1531, the percentage errors of the turbulence models increase. The SA turbulence model of Spalart-Allmaras [40] presents the best fit with the experimental pressure data, with percentage errors below 10%.

The standard $k-\varepsilon$ turbulence models of Launder and Spalding [24], RNG $k-\varepsilon$ of Orszag et al. [38], standard $k-\omega$ of Wilcox [25], SST $k-\omega$ of Menter [27], and RSM of Launder et al. [39] present higher percentage errors with respect to the SA turbulence model. The magnitude of the sum of squared error is also 76.43, which is lower than the other turbulence models evaluated.

In references C and G, the pressures are kept constant for the different pressure ratios r_p; there, the curves of the pressure patterns intersect. In reference D of the throat section, the pressure drops increase as the pressure ratio r_p increases. At the vertices of the straight-cut throat end walls, pressure drops are present and are of greater magnitude for flow at the throat entrance. For flow with r_p = 1.1531, the pressure is close to vacuum pressure.

For future work, for the case of the Venturi tube, we will simulate the incompressible flow field in 3D domains by FVM and FEM for different turbulence models and compare it with 2D domains in order to determine which of the two computational domains present lower numerical errors.

REFERENCES

[1] Invention of the Venturi meter, *Nature,* No. 136, p. 254, 1935, https://doi.org/10.1038/136254a0.

[2] Cengel, Y.A. and Cimbala, J.M.: *Fluid Mechanics Fundamentals and Applications,* McGraw-Hill, 2006.

[3] Stauffer, T.B., Johnson, M.C., Sharp, Z.B. and Barfuss, S. L.: Multiple tap sets to improve Venturi flowmeters performance characteristics with disturbed flow, *AWWA Wat Sci.*, el 134, pp. 1-9, 2019, https://doi.org/10.1002/aws2.1134.

[4] Ulas, A.:*Flow Measurement and Instrumentation*, Vol. 17, No. 2, p.93, 2006.

[5] Itano, E., Shakal, A., Martin, J. and Shears, D.: SAE Technical Paper961730, 1996.

[6] Bean, H.S.: *Fluid meters their theory and applications*, 6 ed., ASME, Tech. Rep., 1971,

[7] Tolentino, S.L.: Experimental and numerical study of the pressure of the water flow in a Venturi tube, *INGENIUS,* No. 23, pp. 9-22, 2019, https://doi .org/10.17163/ings.n23.2020.01.

[8] Long, X., Zhang, J., Wang, J. Xu., M., Lyu, Q. and Ji, B.: Experimental investigation of the global cavitation dynamic behavior in a Venturi tube with special emphasis on the cavity length variation, *International Journal of Multiphase Flow,* Vol. 89, pp. 290-298, 2017, http://dx.doi.org/10.1016/j. ijmultiphaseflow.2016.11.004.

[9] Lindley, D.: An experimental investigation of the flow in a classical venturimeter, *Thermodynamics and Fluid Mechanics Group*, Vol. 184, No. 1, pp. 133-145, 1969, https://doi.org/10.1243/PIME_PROC_1969_184_015_02.

[10] Dudzinski, T.J., Johnson, R.C. and Krause, L.N.: Venturi meter with separable diffuser, *Journal of Basic Engineering, Transactions of the ASME*, pp. 116-120, 1969.

[11] Tukimin, A., Zuber, M. and Ahmad, K.A.: CFD analysis of flow through Venturi tube and its discharge coefficient, *AEROTECH VI-Innovation in Aerospace Engineering and Technology, Conf. Series: Materials Science and Engineering,* Vol 152, 2016, https://doi.org/10.1088/1757-899X/152/1/012062.

[12] Kim, Y.K., Lee, D.Y. H.D. Kim, A., J. H and Kim, K.C.: An experimental and numerical study on hydrodynamic characteristics of horizontal annular type water-air ejector, Vol. 26, No. 9, pp. 2773-2781, 2012, https://doi.org/10.1007/s12206-012-0724-9.

[13] Zhan, J., Yuan, W., Chen, Z. and Wang, Z.: Experimental and numerical study on the drainage performance and fluid flow of Venturi tubes, *AIP Advances,* Vol.9, pp. 065003 1-9, 2019, https://doi.org/10.1063/1.5099420.

[14] Lee, C.H., Choi, H., Jerng, D.W., Kim, D.E., Wongwises, S. and Ahn, H.S.: Experimental investigation of microbubble generation in the Venturi nozzle, *International Journal of Heat and Mass Transfer*, Vol. 136, pp. 1127-1138, 2019, https://doi.org/10.1016/j.ijheatmasstransfer.2019.03.040.

[15] Tomov, P., Khelladi, S., Ravelet, F., Sarraf, C., Bakir, F. and Vertenoeuil, p.: Experimental study of aerated cavitation in a horizontal Venturi nozzle, *Experimental Thermal and Fluid Science*, *Elsevier*, Vol. 70, pp. 85-95, 2016, https://hal.archivesouvertes.fr/hal-01176675v2.

[16] Schlichting, H. and Gersten, K.: *Boundary-layer theory*, 9 ed., Berlin Heidelberg, Germany, Springer Verlag, 2017.

[17] Reynolds, O.: An experimental investigationof the circumstances which determine whetherthe motion of water shall be direct or sinuous,and of the law of resistance in parallel channelsauthor(s): Osborne Reynolds, *PhilosophicalTransactions of the Royal Society of London*,Vol. 174, pp. 935–982, 1883.

[18] Zhang, X., Wang, D., Liao, R., Zhao, H. and Shi, B.: Study of mechanical choked Venturi nozzles used for liquid flow controlling, *Flow Measurement and Instrumentation*, Vol. 65. pp. 158-165, 2019, https://doi.org/10.1016/j.flowmeasinst.2018.12.001.

[19] Wang, J. Wang, L. Xu., S., Ji., B. Long, X.: Expe–rimental investigation on the cavitation perfor–mance in a Venturi reactor with special emphasis on the choking flow, *Journal Experimental Ther–mal and Fluid Science,* Vol. 106, pp. 215-225, 2019, https://doi.org/10.1016/j.expthermflusci.2019.05.003.

[20] Kozák, J., Rudolf, P., Hudec, M., Stefan, D. and Forman, M.: Numerical and experimental investigation of the cavitating flow within Venturi tube, *Journal of Fluids Engineering,* Vol. 141, pp. 041101 1-9, 2019.

[21] Brinkhorst, S, von Lavante, E. and Wendt, G.: Experimental and numerical investigation of the cavitation-induced choked flow in a Herschel Venturi-tube, *Flow Measurement and Instrumentation,* Vol. 54, pp. 56-67, 2017, http://dx.doi.org/10.1016/j.flowmeasinst.2016.12.006.

[22] Ferziger, J.H., Perić, M. and Street, R.L.: *Computational Methods for Fluid Dynamics*, 4 ed., Springer, 2020.

[23] ANSYS, Ansys Fluent 12.0 Theory guide. https://www.afs.enea.it/project/neptunius/docs/fluent/html/th/main_pre.htm

[24] Launder, B.E. and Spalding, D.B.: Lecturesin mathematical models of turbulence, A. P.London, New York, Ed., 1972.

[25] Wilcox, D.C.: Reassessment of the scale determining equation for advanced turbulence models, *AIAA Journal*, vol. 26, no. 11, pp. 1299–1310, 1988, https://doi.org/10.2514/3.10041.

[26] Tolentino, S.L., González, O. and Mírez, J.: Comparative evaluation of DES and SAS turbulence models for incompressible flow in a tube Venturi, *INCAS Bulletin*, Vol. 14, No. 2, pp. 87-101, https://doi.org/10.13111/2066-8201.2022.14.2.8.

[27] Menter, F.: Two equation eddy-viscosity Turbulence models for engineering applications, *AIAA Journal*, Vol. 32, pp. 1598-1605, 1994, https://doi.org/10.2514/3.12149.

[28] Sun, Y. and Niu, W.: Simulating the effects of structural parameters on the hydraulic performances of Venturi tube, *Modeling and Simulation in Engineering*, Vol. 2012, Article ID 458368, pp. 1-7, 2012, https://doi.org/10.1155/2012/458368.

[29] Youling, X., Xiwei, W., Jiaqiang, Z. and Fengfang, Z.: Simulation and experiment on agricultural chemical mixing process for direct injection system based on CFD, *Transactions of the CSAE*, Vol. 26, No. 5, pp. 148-152, 2010,https://doi.org/10.3969/j.issn.1002-6819.2010.05.026.

[30] Reader, M.J., Brunton, W.C., Gibson, J.J., Hodges, G. and Nicholson, I.G.: Discharge coefficients of Venturi tubes with standard and non-standard convergent angles, *Flow Measurement and Instrumentation*, Vol. 12, pp. 135-145, 2001.

[31] Novković, D.M., Lečić, M.R., Burazer, J.M. and Radenković, D.R.: Flow simulations in a small bulb turbine using two-equation turbulence models, *FME Transactions*, Vol. 42, No. 2, pp. 118-127, 2014.

[32] Gumen, O., Dovhaliuk, V., Mileikovskyi, V., Lebedieva, O., and Dziubenko, V.: Geometric analysis of turbulent macrostructure in jets laid on flat surfaces for turbulence intensity calculation, *FME Transactions*, Vol. 45, no. 2, pp. 236-242, 2017.

[33] Dovhaliuk, V., Gumen, O., Mileikovskyi, V., and Dziubenko, V.: Simplified analysis of turbulence intensity in curvilinear wall jets, *FME Transactions*, Vol. 46, No. 2, pp. 177-182, 2018.

[34] Jemcov, A. Gonzales, J.P., Maruszewski, V., and Kelli, R.T.: Non-iterative wall model formula for non-equilibrium boundary layer flows, *FME Transactions*, Vol. 50, no. 2, pp. 223-237, 2022.

[35] Mirkov, N., Stevanović, Ž., Stevanović, Ž.: Turbulence Model of Atmospheric Boundary Layer in General Curvilinear Coordinate System, *FME Transactions*, Vol. 36, No. 4, pp. 151-156, 2008.

[36] Tolentino, S.L.: Evaluation of turbulence models for the air flow in a planar nozzle, *Ingenius,* No. 22, pp. 25-37, 2019, https://doi.org/10.17163/ings.n22.2019.03.

[37] Tolentino, S.L.: Evaluation of turbulence models for the air flow in a transonic diffuser, *Polytec–hnicJournal*, Vol. 45, No. 1, pp. 25-38, 2020. (In Spanish).

[38] Orszag, S.A et al.: Renormalization Group Mode–ling and Turbu–lence Simulations*, In International Conference on Near-Wall Turbulent Flows, Tempe, Arizo–na*. 1993.

[39] Launder, B.E., Reece, G.J. and Rodi, W.: Progress in the development of a Reynolds-stress turbulence closure,*Journal of Fluid Mechanics,* Vol. 68, No. 3, pp. 537-566, 1975, https://doi.org/10.1017/s0022112075001814.

[40] Spalart, P.R. and Allmaras, S.R.: A one-equation turbulence model for aerodynamic flows, in: *30th Aerospace Sciences Meeting and Exhibit, 06 January 1992 – 09*, Reno, NV, U.S.A, 1992, pp. 1-22, https://doi.org/10.2514/6.1992-439.

NOMENCLATURE

L_i	Venturi tube length cross-section
L_t	Total length of Venturi tube
p_{exp}	Pressure from experimental data
p_{sim}	Pressure from computational simulations
p_{inlet}	Inlet pressure
p_{outlet}	Outlet pressure
r_p	Pressure ratio
y^+	y-plus, in the shear stress value
x/L_t	Position, distance relation
FDM	Finite difference method
FEM	Finite element method
FVM	Finite volume method

ПРОЦЕНА МОДЕЛА ТУРБУЛЕНЦИЈЕ ЗА НЕСТИШЉИВ ТОК У ВЕНТУРИЈЕВОЈ ЦЕВИ

С.Л. Толентино, Х. Мирес, О. Гонзалес

Модели турбуленције су полу-емпиријске транс–портне једначине које моделирају понашање стру–јања. Они се редовно упоређују да би се знало који од њих најбоље одговара експерименталним подацима за различиту лабораторијску опрему. У овом раду, поље нестишљивог струјања (вода) је симулирано помоћу алата за рачунарску динамику флуида (ЦФД) и РАНС модела за геометрију Вентуријеве цеви у 2Д рачунарским доменима, са циљем да се процени шест модела турбуленције: стандардни к- ε, РНГ к-ε, стандардни к-ω, ССТ к-ω, РСМ и СА. Нумерички резултати трајекторија криве обрасца притиска на зидовима и аксијалне симетрије су блиски једни другима. На грлу долази до пада притиска.

Процентуалне грешке модела турбуленције расту како се повећава величина односа притисака, за r_p = 1,0932, r_p = 1,1118, r_p = 1,1377 и r_p = 1,1531. Закључено је да модел СА турбуленције Спаларт-Алмарас (1992) најбоље од–говара експеримен–талним подацима о притиску, са процентуалним грешкама мањим од 10%.